A super Asian dust storm over the East and South China Seas: Disproportionate dust deposition

Shih-Chieh Hsu,[1] Fujung Tsai,[2] Fei-Jan Lin,[3] Wei-Nai Chen,[1] Fuh-Kwo Shiah,[1] Jr-Chuan Huang,[4] Chuen-Yu Chan,[5] Chung-Chi Chen,[6] Tsun-Hsien Liu,[7] Hung-Yu Chen,[2] Chun-Mao Tseng,[3] Gwo-Wei Hung,[8] Chao-Hao Huang,[1] Shuen-Hsin Lin,[1] and Yi-Tang Huang[1]

[1]   A super Asian dust (SAD) storm that originated from North China has affected East Asia since 20 March 2010. The tempo-spatial and size distributions of aerosol Al, a tracer of wind-blown dust, were measured on a regional aerosol network in March 2010. Two dust events were recorded: the SAD and a relatively moderate AD event. The SAD clouds raised Al concentrations to ~50 µg/m^3 on 21 and 22 March over the East China Sea (ECS) and occupied there for ~5 days. The SAD plume also stretched toward the South China Sea (SCS) on 21 March however, it caused a maximum Al concentration of ~8.5 µg/m^3 only, much lower than that observed in the ECS. In comparison, a weaker dust plume on 16 March caused Al maximum of ~4 µg/m^3 over the ECS, and comparably, ~3 µg/m^3 in the SCS. Dry dust deposition was measured during the peak phase of the SAD at 178 mg/m^2/d, which corresponded to dry deposition velocities of 0.2–0.6 cm/s only, much lower than the commonly adopted one (1–2 cm/s). The corresponding increase in dust deposition by the SAD was up to a factor of ~12, which was, however, considerably disproportionate to the increase in dust concentration (i.e., the factor of over 100). In certain cases, synoptic atmospheric conditions appear to be more important in regulating dust contribution to the SCS than the strength of AD storms.

1. Introduction

[2]   Asian dust (AD) storms occur annually in late winter and spring over West and North China [*Wang et al.*, 2000; *Zhang et al.*, 2003a]. There are two main AD sources, namely, the Gobi deserts in northern China and Mongolia, and the Taklamakan Desert in western China [*Sun et al.*, 2001; *Zhang et al.*, 2003a, 2003b]. The highest frequency (58%) of dust storm occurrence in the Gobi deserts is in the April [*Sun et al.*, 2001], which is slightly different from the case in Taklamakan Desert, wherein dust storms frequently occur in April to July [*Wang et al.*, 2005]. Massive quantities of AD can be entrained into the free troposphere and then brought by the prevailing westerlies, traveling thousands of kilometers or more from source regions to neighboring countries, such as Korea and Japan [*Choi et al.*, 2001; *Uematsu et al.*, 2002; *Trochkine et al.*, 2003; *Uno et al.*, 2008], the North Pacific [*Duce et al.*, 1980; *Gao et al.*, 1992, 1997; *Husar et al.*, 2001], and North America [*VanCuren and Cahill*, 2002]. *Laurent et al.* [2006] recently estimated the emission of dust from the Chinese and Mongolian deserts between 100 and 460 Mt/yr compared with the earlier estimate of ~800 Mt/yr by *Zhang et al.* [1997]. Of the latter amount, 30% is redeposited around the dust sources, and 50% is carried downwind to the oceanic regions [*Zhang et al.*, 1997]. Around East China, such as the Yangtze River Delta and the East China Sea (ECS), AD may be subject to the regime of the northeastern monsoon, usually following a frontal system. The AD transported southeastward to Taiwan is carried by the prevailing northeasterly monsoon winds within a thin layer, usually below 1.5 km [*Chen et al.*, 2004; *Hsu et al.*, 2004, 2008, 2009a; *Liu et al.*, 2009] and as far as Hong Kong

[1]Research Center for Environmental Changes, Academia Sinica, Taipei, Taiwan, ROC.
[2]Department of Marine Environmental Informatics, National Taiwan Ocean University, Keelung, Taiwan, ROC.
[3]Institute of Oceanography, National Taiwan University, Taipei, Taiwan, ROC.
[4]Department of Geography, National Taiwan University, Taipei, Taiwan, ROC.
[5]Division of Engineering, The University of Nottingham Ningbo China, Ningbo, Zhejiang Province, China.
[6]Department of Life Science, National Taiwan Normal University, Taipei, Taiwan, ROC.
[7]Center for Environmental Studies, National Central University, Jhongli, Taoyuan, Taiwan, ROC.
[8]Center for General Education, National Penghu University of Science and Technology, Penghu, Taiwan, ROC.

Corresponding author: S. C. Hsu, Research Center for Environmental Changes, Academia Sinica, Taipei, Taiwan, ROC. (schsu815@rcec.sinica.edu.tw)

[*Fang et al.*, 1999; *Wai and Tanner*, 2005] and the South China Sea (SCS) [*Lin*, 2007; *Wang et al.*, 2011], where AD have not well been simulated in model studies at times [*Zhao et al.*, 2003; *Park et al.*, 2011]. For example, *Park et al.* [2011] have modeled monthly mean PM_{10} concentrations for the ECS and SCS to be 24.7 and only $1.4\,\mu g/m^3$ in March 2010, respectively, which are rather small as compared to our observations on two islands (i.e., 99 and $21\,\mu g$ dust/m^3, respectively), which is to be shown later. The main dust sources that influence the southern ECS and Taiwan have been identified to be around Badam-Julin Desert [*Hsu et al.*, 2008; *Liu et al.*, 2009].

[3] Dust aerosols are often associated with pollutant species and, thus, can deteriorate air quality and pose risks to public health [*Chou et al.*, 2004; *Hsu et al.*, 2005, 2006, 2009b; *Chi et al.*, 2008; *Wu et al.*, 2010]. Likewise, dust aerosols can profoundly affect the Earth's climate through direct and indirect influence on the radiation balance of the atmosphere [*Tegen et al.*, 1996; *Chen et al.*, 2010]. Atmospheric deposition of Fe in dust aerosols has been well recognized as a primary source of bioavailable Fe to the open oceans [*Gao et al.*, 2001; *Mahowald et al.*, 2005], closely linking to oceanic production and in turn carbon sequestration, particularly in the high-nitrate low-chlorophyll regions [*Jickells et al.*, 2005]. It is further hypothesized that the enhanced dust (in turn Fe) supply to the open oceans during the glacial ages plays a vital role in reducing CO_2 in the atmosphere at that time [*Martin*, 1990]. Moreover, AD has been known to serve as a main source of pelagic sediments over the North Pacific, and thus its variability in cored sediments is often applied as a proxy of paleoclimate [*Rea*, 1994]. Actually, it has been observed that AD conveyed bioavailable iron to the northwestern North Pacific, hence stimulating production [*Iwamoto et al.*, 2011]. Phytoplankton in the Kuroshio Current flowing around the East China Sea continental shelf break can mitigate the demand pressure for iron, phosphorus, and nitrogen during an AD event [*Chung et al.*, 2011]. AD is also suggested to enhance nitrogen fixation in the oligotrophic waters of the North Pacific [*Wong et al.*, 2002; *Wu et al.*, 2003]. The biogeochemical effects of AD deposition are closely related to carbon sequestration [*Bishop et al.*, 2002], which might mitigate global warming.

[4] Most modeling studies have presumed that dust (and dust-associated iron) deposition to the oceans is considerably episodic in nature and event-dependent [*Aumont et al.*, 2008]. Meanwhile, few field measurements that use observational evidence can support the validity of such claims, particularly for episodically severe dust storms. Numerical model investigations can yield a wide range of results on dust concentrations and deposition fluxes [*Todd et al.*, 2008], whereas model simulation proves to be a powerful approach [*Mahowald et al.*, 2009]. Aerosol optical depth (AOD) retrieved from satellite remote sensing has been utilized as alternative means to evaluate atmospheric deposition over the oceans [*Jurado et al.*, 2004; *Singh et al.*, 2008] that, in turn, can be used to assess the impact of eolian dust on marine ecosystems [*Gao et al.*, 2001; *Lin et al.*, 2007, 2009, 2011; *Shaw et al.*, 2008]. Nevertheless, investigations have found inconsistencies among satellite retrievals, model simulations and observations [*Mahowald et al.*, 2005], thus requiring precaution and verification [*Mahowald et al.*, 2009]. Accordingly, comprehensive field measurements are urgently needed to reduce the

uncertainties and thereby improve the performance of model simulation and remote-sensing retrieval [*Prospero et al.*, 2010].

[5] AD has been postulated as a major iron source for the SCS to fertilize the nitrogen fixer *Trichodesmium*, thus enhancing nitrogen fixation [*Wu et al.*, 2003; *Wong et al.*, 2002] and phytoplankton growth [*Wang et al.*, 2012]. Despite the identification of AD in a number of case studies in southeastern China and over the SCS [*Lin*, 2007; *Zhao et al.*, 2011; *Wang et al.*, 2011], extensive aerosol observation has not been conducted in this region, unlike the ECS, in where AD has been periodically observed. AD transport processes over the wide Chinese marginal seas remain unclear, particularly in terms of demonstration from field measurements on a regional scale. A super Asian dust (SAD) storm developed over the Gobi Desert in North China and then struck the entire East Asian region on 20 March 2010 [*Li et al.*, 2011; *Park et al.*, 2011; *Lin et al.*, 2012], which can be readily identified by the spatial distribution of the Moderate Resolution Imaging Spectroradiometer (MODIS) total AOD and natural-color images from both Terra and Aqua satellites [*Liu et al.*, 2011; *Han et al.*, 2012a, 2012b; *Li et al.*, 2012]. In addition to this SAD, about 5 days before the SAD event, another moderate AD (MAD) event, which is much weaker than the SAD, was also transported toward the region under investigation. The two AD cases, which have considerably different strengths, can exemplify the assessment of synoptic atmospheric circulation patterns and their role in regulating the long-range transport of AD to the SCS, aside from dust strength. Briefly, on the basis of a regional aerosol network [*Hsu et al.*, 2012a, 2012b], the present study aims to characterize the transport pathways and tempo-spatial evolution of AD over the Chinese marginal seas and to explore the controlling factors of the observed dust deposition. Besides, we present high time resolution data on dust deposition which are indeed so limited for the oceanic regions downwind major dust sources, particularly during rare extreme dust storms. Therefore, our results will offer implications for long-range AD transport and deposition.

2. Materials and Methods

2.1. Sampling and Chemical Analyses

[6] We set a Taiwan regional background aerosol (TaiBA) network along the Chinese coastlines and in the marginal seas beyond 30°N, which has four offshore island/coastal stations, as depicted in Figure 1: Pengchiayu (PCY) islet in the southern ECS, Dongsha (DS) island in the northern SCS, Kinmen (KM) island on the Taiwan Strait, and Zhuhai (ZH) on the campus of the University of Sun-Yat-Sen, Guangzhou, near the Pearl River Estuary. By taking advantage of the TaiBA network, we could readily observe the interesting features of the regional and hemispheric transport of air species [*Hsu et al.*, 2012a, 2012b; *Huh et al.*, 2012]. We collected daily total suspended particulate (TSP) aerosol samples from the four stations using high-volume TSP samplers (TE-5170D; Tisch Environmental, Inc.) between 11 and 30 of March 2010. During the said interval, two AD events occurred: one between 15 and 16 of March and another between 21 and 23 of March. A few samples were collected with a 2 day interval. Whatman®41 cellulose filters ($8'' \times 10''$) were used as filtration substrates. Two sets of size-resolved aerosol samples
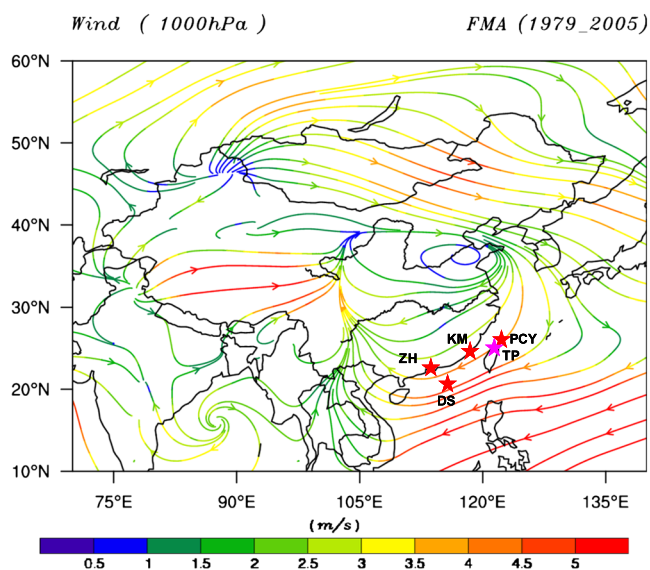
Figure 1. Regional map of four TSP sampling stations (indicated by pink stars), including Pengchiayu (PCY) in the southern East China Sea, Kinmen (KM) in the Taiwan Strait, Zhuhai (ZH) in the Pearl River Delta of Southeast China, and Dongsha (DS) in the northern South China Sea; and the size-resolved aerosol and dry deposition sampling station (indicated by the red star), in Taipei (TP), North Taiwan. The base map shows typical 1000 hPa streamlines during winter/spring (February, March, and April) for 1979–2005. Arrows indicate prevailing wind directions. Color scale indicates wind speed (m/s). Northeasterly monsoon is obvious in the south of 30°N.

were collected in Taipei, northern Taiwan during the course of the SAD (from 17:00 on 22 March 2010 to 17:00 on 24 March 2010, LST) and the ensuing 2 days (from 17:00 on March 24, 2010 to17:00 on March 26, 2010, LST; denoted as the normal case or sample) by using a micro-orifice uniform deposit impactor (MOUDI) sampler (Model 110, MSP Corporation, Minneapolis, Minnesota); Teflon membrane filters (PTFE, 47 mm in diameter and 1.0 μm in pore size, Pall Gelman, East Hills, NY) were used. All filter-laden particles were completely dissolved in an acid mixture by using a microwave digestion system (MARSXpress, CEM, Corporation, Matthews, NC). The digestion solution was subjected to chemical analyses for crustal elements, such as Al and Fe, using a quadrupole-based, inductively coupled plasma mass spectrometer (Elan 6100, PerkinElmer, Waltham, Massachusetts). Here Al served as an indicator of dust, directly representing the dust particles [*Duce et al.*, 1980; *Prospero et al.*, 2003; *Hsu et al.*, 2004, 2008]. Quality assurance and control (QA/QC) of data were validated by the analyses of a standard reference material (National Institute of Standards and Technology SRM-1648, urban particulate), following the same treatment as samples within a recovery of $100 \pm 5\%$ (n = 5). The detection limits of Al and Fe in the TSP samples were at 5 ng/m^3, whereas that of Al in the size-resolved samples was as low as 0.5 ng/m^3. Detailed sampling and analytical methods were provided by *Hsu et al.* [2008, 2009a, 2009b, 2010a, 2010b, 2010c].

[7] We employed a surrogate surface water glass dish (19 cm in diameter and 8.5 cm in depth; SCHOTT DURAN) for collecting the dry deposition of dust particles at the same sampling site of the size-resolved aerosols during the passage

of the SAD plume, along with a routine collection of weekly bulk deposition by using a cylindrical high-density polyethylene tank (30 cm in diameter and 36 cm in depth), principally similar to those used by *Azimi et al.* [2003] and *Inomata et al.* [2009]. These two kinds of containers were infused into 0.10 and 0–1 l (dependent on whether or not raining occurred at the beginning of deployment) of Milli-Q water prior to use, respectively. The recovered water that was loaded with deposited particles was filtrated through a pre-weighed polycarbonate membrane (0.45 mm pore in size and 47 mm in diameter, Nuclepore) by using plastic filtration units (Nalgene Filterware 300–4100), thus representing the insoluble fraction of the collected particles that were assumed to be dominated by the total deposited mineral dust particles (~70–90%) [*Prospero et al.*, 2010]. The insoluble particle loadings were gravimetrically obtained after drying the particle-laden membrane filters.

2.2. AOD and Meteorological Data and Back Trajectory Analyses

[8] In order to explicitly depict the tempo-spatial distribution and evolution of eolian dust loadings in the study region, the total AOD data were used in the present study. Total AOD data with $1° \times 1°$ resolution are the level 3.0 products (at 550 nm wavelength) from Moderate resolution Imaging Spectrometer (MODIS) sensors on board Terra and Aqua satellites. Because there are large blank over East China and the studied marginal oceans on the MAD and SAD days, therefore the composite AOD map on 15–16 and 21–22 March are adopted, as depicted in Figure 2.

[9] The synoptic conditions during the dust event were analyzed based on the National Centers for Environmental Prediction (NCEP)/National Center for Atmospheric Research (NCAR) Reanalysis [*Kalnay et al.*, 1996]. The global reanalysis data have a spatial resolution of $2.5° \times 2.5°$ and a temporal resolution of 6 h, including a three-dimensional wind field and sea-level pressure. In addition, surface dust observations obtained from the World Meteorological Organization (WMO) were used to identify the source of the dust event [*WMO*, 2010]. In the WMO SYNOP (surface synoptic observations) code, the three-hourly weather reports for distinguishing dust intensity from haze to severe dust storm were employed in the present study to identify dust events. Dust observations from more than 800 surface stations in China were included for analysis.

[10] Five-day air mass back trajectories were calculated by using the National Oceanic and Atmospheric Administration (NOAA) Hybrid Single Particle Lagrangian Integrated Trajectory (HYSPLIT) model with a $1° \times 1°$ latitude-longitude grid and the final meteorological database [*Draxler and Rolph*, 2012; *Rolph*, 2012] to explore the likely transport pathways of AD plumes arriving at the four TSP aerosol stations. The six-hourly final archive data were generated from the NCEP Global Data Assimilation System (GDAS) wind field reanalysis. The GDAS uses a spectral medium-range forecast model. Details on the HYSPLIT model can be found at http://www.arl.noaa.gov/ready/open/hysplit4.html, as prepared by the NOAA Air Resources Laboratory. Air mass back trajectory calculations were performed at 500 m because the southeastward transport of AD to the study region is driven by the northeasterly monsoonal circulation and is confined within the 1500 m layer aboveground [*Chen et al.*, 2004; *Liu et al.*, 2009].
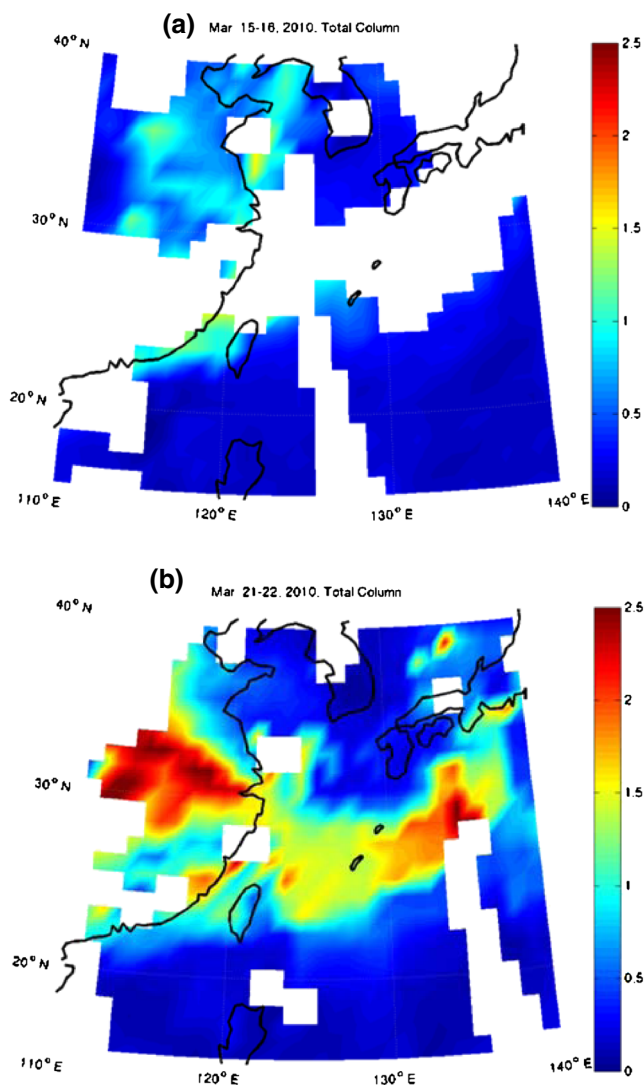
**Figure 2.** Spatial distribution of AOD retrieved from MODIS at 550 nm on (a) 15–16 March and (b) 21–22 March.

3. Results and Discussion

3.1. Regional and Temporal Variation in PM_{10} and Dust-Derived Al Concentration

[11] PM_{10} (PM with an aerodynamic diameter of less than 10 μm) has routinely been monitored with an hourly resolution around Taiwan and Hong Kong. Although composed of various components, such as mineral dust, sulfate, nitrate, ammonium, sea salt, organic matter, and elemental carbon, PM_{10} is usually dominated by mineral dust particles during dust episodes [Hsu et al., 2004, 2008; Chou et al., 2004]. Figure 3 shows the time series of hourly PM_{10} concentrations during the two AD events monitored at selected air-quality stations in Taiwan, under the Environmental Protection Administration (EPA, http://taqm.epa. gov.tw/taqm/zh-tw/) and in Hong Kong, under the Environmental Protection Department (EPD, http://www.epd.gov. hk/epd/english/environmentinhk/air/air_maincontent.html). To determine the arrival time of the SAD at each air-quality monitoring station, we identified the time when the PM_{10} hourly concentration at a given hour increased by 50% more

than the average concentration in the earlier 3 h, and then we designated such time as the arrival time of the SAD at a selected station. The arrival times are indicated by arrows on the x axes (time) of the three panels in Figure 3. Based on the results, we determined the time at the TSP sampling sites: earlier than 03:00 LST on 21 March at PCY (based on the time of Station Wanli); 07:00 LST on 21 March at KM; and 20:00 LST at ZH (based on the time of Station Tungyong, Hong Kong). With regard to the results of Wang et al. [2011], the arrival time of the SAD was determined to be 20:00 LST on 21 March similar to that of ZH. Hourly PM_{10} concentrations dramatically increased and then reached a maximum of more than 1000 μg/m^3 in northern Taiwan and the Taiwan Strait, namely, stations Wanli and Penghu (Figure 3).

[12] Figure 4 shows the time series of the Al concentrations at our TaiBA network stations: PCY, DS, KM, and ZH. The data represent the mean concentration averaged through 1 day (or 2 days for several samples) from one morning to the succeeding morning. We used the sampling beginning date as a tick label of the x axis in Figure 4. Therefore, when addressing the arrival time of the dust plumes determined from the time series of PM_{10} concentrations, the dates may not be the same as those shown in Figure 4. Aluminum concentrations at PCY reached 47221 ng/m^3 on 20 March and 51118 ng/m^3 on 21 March, which corresponded to daily dust concentrations of almost 700 ± 30 μg/m^3 when assuming Al content (~7%) in dust aerosols similar to that in the Chinese desert and loess dust [Zhang et al., 2003a]. The magnitude was found to be consistent with the levels of hourly PM_{10} (>1000 μg/m^3) monitored by Taiwan EPA on Taiwan's northern tip (Wanli) during the peaking phase of the SAD (Figure 3). Such PM_{10} levels (~1200 μg/m^3) were measured in the downwind Sado, Japan in March 2002 [Han et al., 2004]. However, the daily maximum concentration of PM_{10} monitored in Beijing during the peaking phase of the SAD was only ~800 μg/m^3 on 20 March [Li et al., 2011; Liu et al., 2011], which was lower than those extensively monitored around Taiwan (Figure 3) [Lin et al., 2012]. One of the most likely reasons is that the values of daily PM_{10} concentrations presented by Liu et al. [2012] were converted from ground API (air pollution index) values, instead of the real monitoring PM_{10} data. Following the maxima, Al concentrations remained at a high level of ~10,000 ng/m^3 in the ensuing 2 days at PCY. Extraordinary Al levels were observed at KM and ZH, Southeast China, at 52,526 and 37,805 ng/m^3, respectively. Despite the peaking times on 21 and 22 March, respectively, no sample was available from ZH for 21 March. Thus, the arrival time of dust clouds lagged for several hours, and the influencing time was shortened relative to PCY; the magnitudes of the maximum concentrations were thus comparable. Unexpectedly, the spiking Al concentration observed on the DS islet was only 8509 ng/m^3 on 21 March, which was incomparable with that measured at ZH, although the arrival times of the SAD plumes at DS and ZH were the same on late 21 March (20:00 LST) (Figure 3). Briefly, the influencing times were between 4 and 5 days at PCY, between 1 and 2 days at KM and ZH, and less than 1 day at DS. With consideration for the entire influencing time at each site, the difference in Al abnormal concentrations among the four sites would be amplified. Thus, this
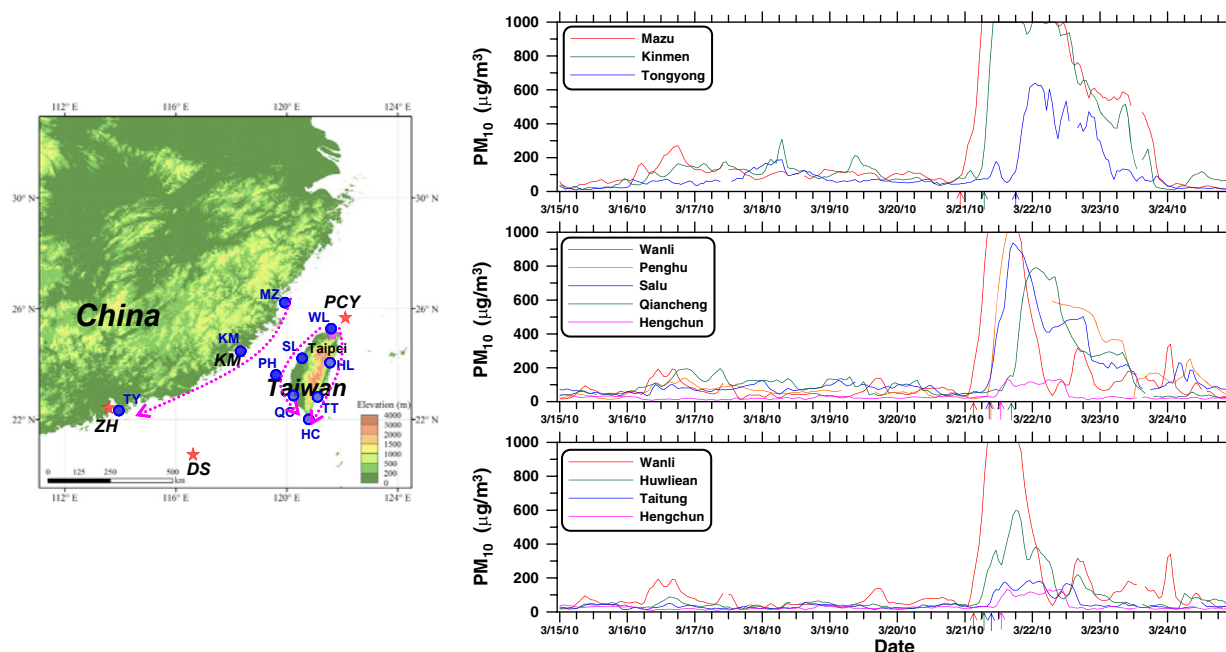
Figure 3. Regional map (left panel) of air-quality stations (blue solid circles) along with aerosol sampling stations (red and pink stars). Also shown is the time series of PM_{10} hourly concentrations (in $\mu g/m^3$; three right panels) along three transects (dashed curved, pink arrows) between 15 and 24 March 2010. The left transect represents the area along the Southeast Chinese coastlines, including the Matzu (MZ), Kinmen (KM), and Tongyong (TY, Hong Kong) stations, where PM_{10} time series data are shown on the right-upper panel. The middle transect denotes the area along west Taiwan, including the Wanli (WL), Salu (SL), Penghu (PH), Qiangcheng (QC), and Hengchun (HC) stations, whose PM_{10} time series data are shown on the right-middle panel. The right transect is along east Taiwan, including the WL, Huwliean (HL), Taitung (TT), and HC stations, whose time series data are shown on the right-lower panel. Among these stations, two (WL and HL) are repeated in the middle and right transects, respectively, so that the northern and southern ends of Taiwan can be compared. Data for all stations were mainly obtained from the Taiwan Environmental Protection Administration (EPA; http://taqm.epa.gov.tw/taqm/en/Default.aspx), except those of Tongyong, which were obtained from the Hong Kong Environmental Protection Department (EPD; http://www.epd.gov.hk/epd/english/environmentinhk/air/air_maincontent.html). The upper limit of the PM_{10} concentration was initially set at $1000 \, \mu g/m^3$ at most of Taiwan's air-quality network stations. Thus, the maximum concentrations of MZ, KM, WL, and PH should be higher than $1000 \, \mu g/m^3$. The maximum hourly PM_{10} concentration measured in the Shilin District, in Taipei City, at that time, was $1720 \, \mu g/m^3$.

SAD plume might have substantially affected the ECS, resulting in a sharp gradient of dust concentrations within the marine boundary layer across the oceanic region studied, which is very correspondent with the spatial pattern of total AOD (Figure 2b). Larger AOD values of 1.2 to 2.0 were observed over the ocean off northeast Taiwan, whereas about 0.5 was observed over the northern SCS.

[13] Prior to the occurrence of the SAD, a MAD episode, which caused an Al maximum concentration of $3945 \, ng/m^3$, was reported at PCY on 15 March 2010, based on a concentration criterion ($2800 \, ng/m^3$) of an AD event [*Hsu et al.*, 2008]; however, results much lower than those of the SAD were determined. This AD episode might have elevated the Al concentrations at KM to as high as $5649 \, ng/m^3$ on 16 March although this could be partly attributed to anthropogenic sources from its northeastern areas, particularly from ceramic industries [*Hsu et al.*, 2010a]. However, no sample was collected at ZH before 19 March. The earlier MAD plume arrived at DS, which increased the Al concentrations to 3524 and $2690 \, ng/m^3$ on 16 and 17 March 2010, respectively. Compared with the SAD that has resulted in a large difference

in Al maxima between PCY and DS (a ratio of 6.0; when considering the influencing time, the ratio would reach 15 or more), the difference is relatively much smaller (i.e., a ratio of only 1.1). This indicates that the spatial distribution of dust over the study region during the MAD was considerably even, which is also in concert with the spatial distribution of MODIS AOD, showing AOD values around 0.5–1.0 over the southern ECS and the northern SCS (Figure 2a). The distinct meteorological conditions that regulated the transport of the two AD plumes to the ECS and SCS are discussed below.

3.2. Synoptic Conditions Controlling the Southeastward Transport of AD

[14] Figure 5 shows the surface weather maps and the dust observations of the two dust storms during the sampling period. For the MAD case, Figures 5a and 5b show that the dust storm started on 15 March when a cyclonic system passed through eastern Mongolia and northeastern China. Several hours later, dust was generated over northeastern China due to strong surface winds from the intense pressure
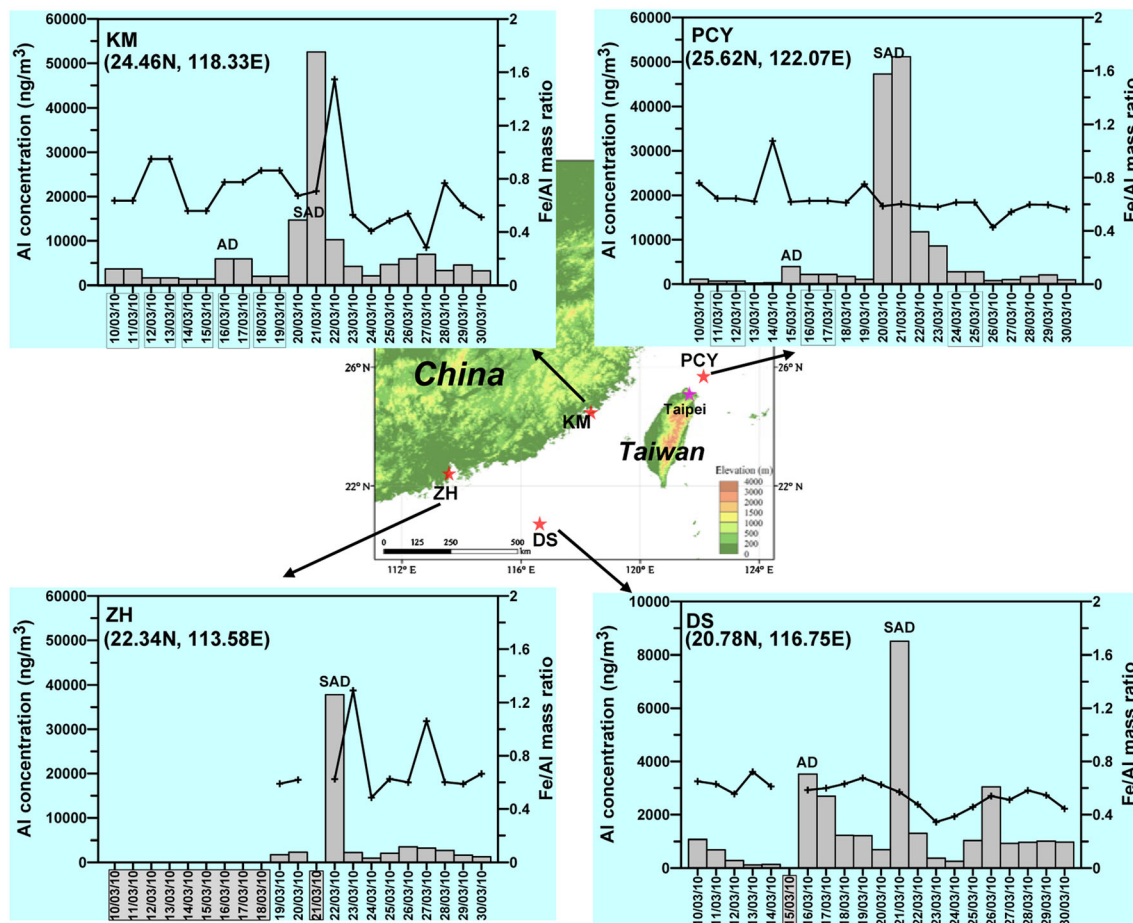
Figure 4. Time series of Al concentrations ($y1$ axis; bars) and Fe/Al mass ratios ($y2$ axis; lines and symbols) in aerosols, between 10 and 30 March 2010, measured at the four TSP stations. The $y1$ axis scale in the DS graph is different from the three other graphs. X axis indicates the start date of sampling of each sample. The label marked by the grayed box indicates that no sample was collected during that date. A few samples were collected at 2 day duration, as marked by the blank box.

gradient between the surface cyclone and anticyclone. In the evening of 15 March, when the associated anticyclone moved southeastward to the eastern coast of China (indicated by H in Figure 5c), dust clouds were also transported ahead of the anticyclone to Korea. On the following day, the northerlies ahead of the anticyclone remained up to 15 m/s. Following the strong northerlies, widespread dust clouds continued to move southward to the southern ECS and Taiwan (Figures 5d and 2a).

[15] For the SAD case, Figures 5e to 5h show that the dust storm began on 19 March, when a cyclonic system passed through Mongolia and northern China. The area with intense pressure gradients between the surface cyclone and the anticyclone obviously covered a wide range of the Gobi desert. The surface winds that resulted from the intense pressure gradient reached 20 m/s, which was considerably stronger than the MAD winds at 10 m/s (Figure 5e). Due to the strong surface winds, the generated dust clouds became widespread (Figure 5f). Two days later, when the surface anticyclone moved southeastward from Mongolia to Shanghai City (about 121°E, 31°N), substantial dust clouds were also transported by the prevailing winds ahead of the anticyclone to the eastern coast (Figures 5g and 5h).

[16] During downwind transport, the locations of the surface anticyclone in the two dust events were characterized by distinct features. In the MAD event, the associated surface anticyclone moved to southeastern China after dust generation, reaching far south beyond 30°N on 16 March (Figures 5d and 2a). The anti-circulation on the surface covered the entire eastern China, and the strong northerlies to northwesterlies ahead of the anticyclone prevailed from northeastern to southeastern China. The strong prevailing winds were favorable for the southward transport of dust to the coastal areas off southeastern China. In contrast, the associated surface anticyclone of the SAD event moved to the eastern coast after dust generation (Figures 5h and 2b). Anti-circulation with weaker prevailing winds occupied a smaller area of the eastern coast of China and northern Taiwan. Although dust generation was much stronger during the SAD, the smaller anti-circulation with weaker prevailing winds limited the southward transport of dust. Such synoptic conditions seemed favorable for the southeastward dispersion of the SAD to the open western Pacific than for the straight southward dispersion to the SCS (Figure 2b), as supported by the CALIPSO lidar data (depolarization ratio) published by *Lin et al.* [2012; seen in their Figure 6].
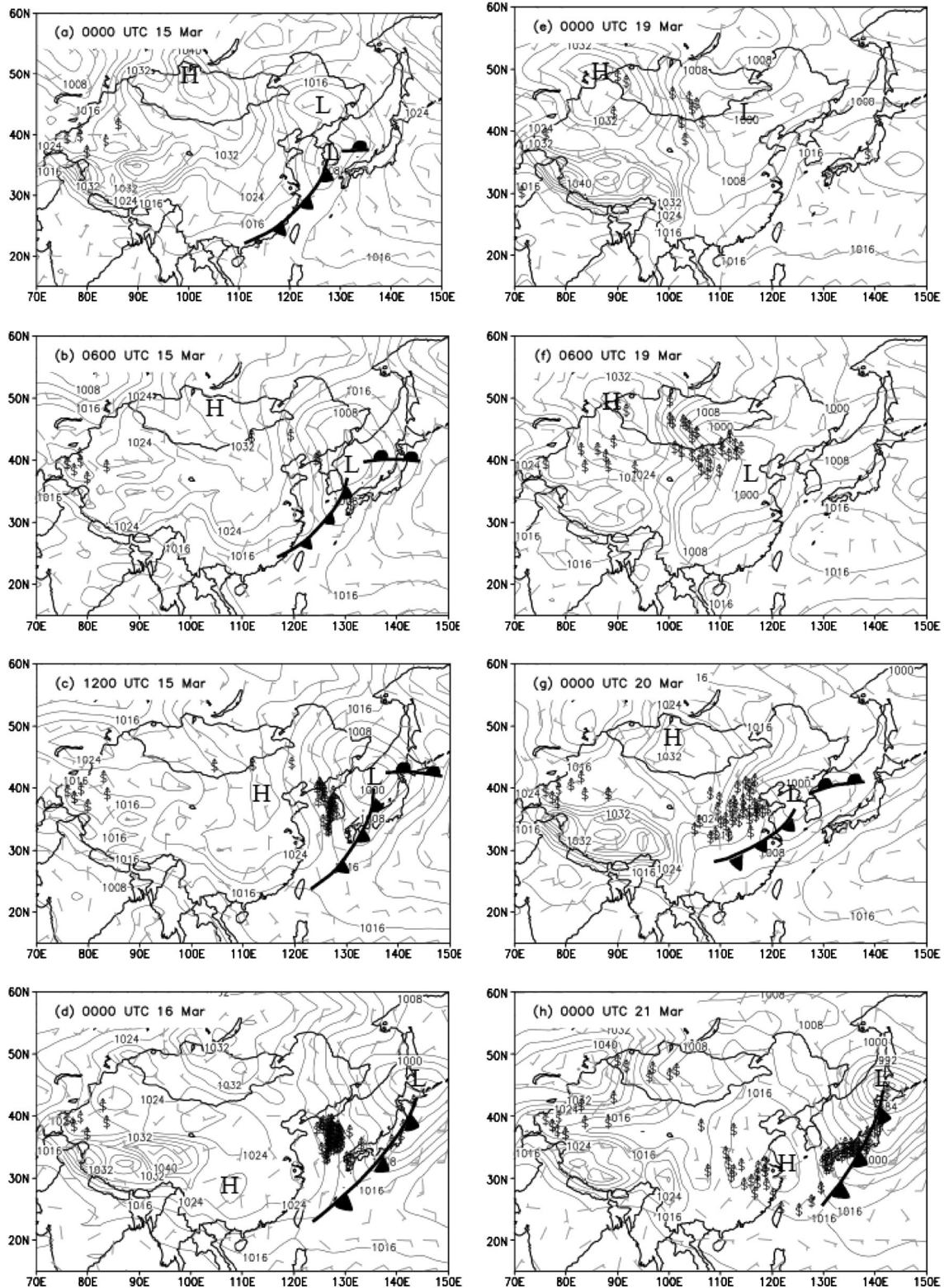
Figure 5. Surface weather map at (a) 0000 UTC on 15 March; (b) 0600 UTC on 15 March; (c) 1200 UTC on 15 March; (d) 0000 UTC on 16 March during the MAD event, and at (e) 0000 UTC on 19 March; (f) 0600 UTC on 19 March; (g) 0000 UTC on 20 March; (h) 0000 UTC on 21 March during the SAD event. Sea-level pressure obtained from NCEP-NCAR Reanalysis was analyzed at 4 hPa intervals. The full barb and half barb were 10 and 5 m s^{-1}, respectively. The High (H) and Low (L) pressure systems and the front (thick line with triangle) and dust observations ($) are marked.
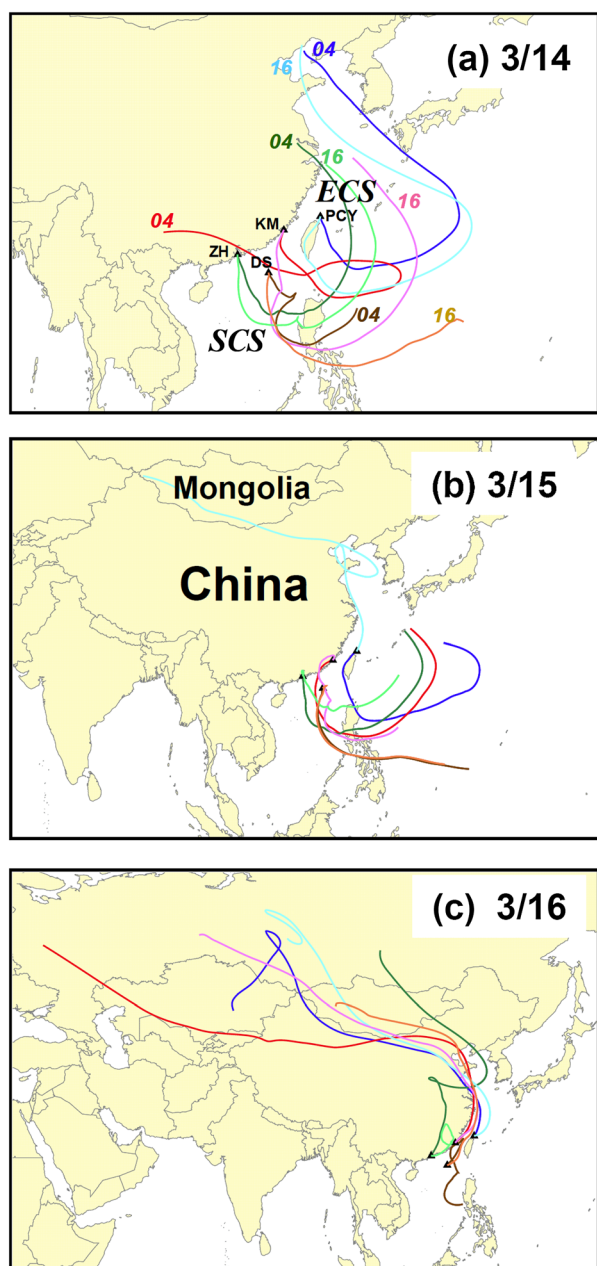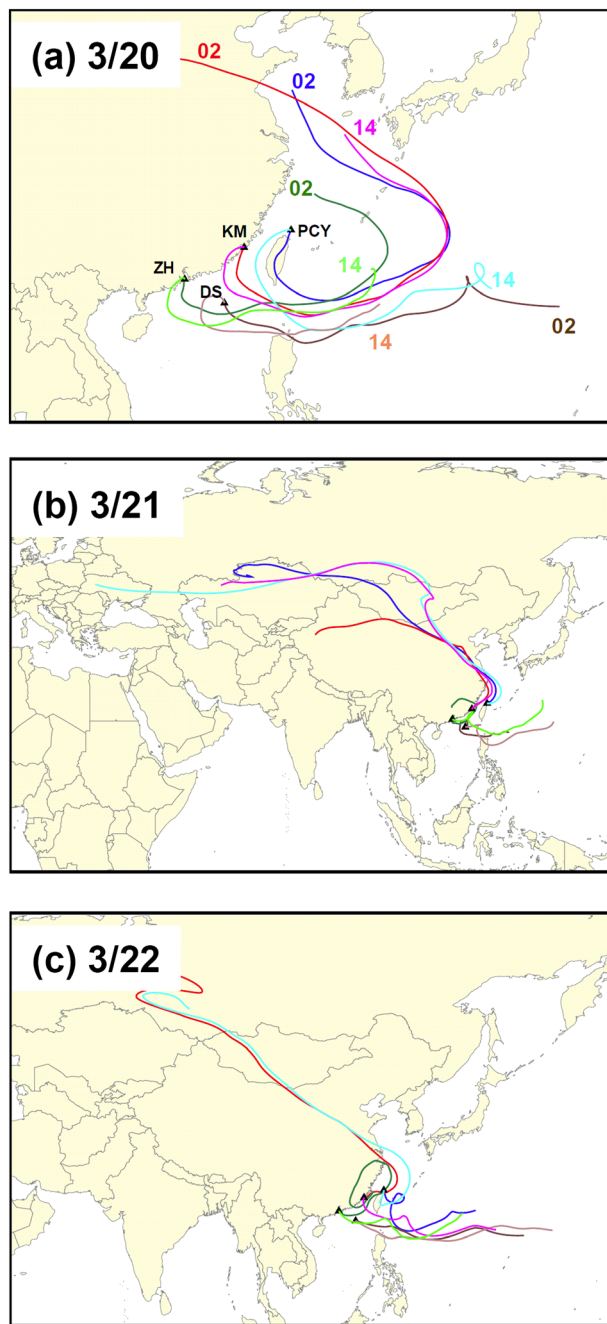
Figure 6. (a–c) The NOAA HYSPLIT modeled 5 day backward trajectories at 500 m starting from the four TSP sampling stations (PCY, KM, ZH, and DS) between 14 and 16 March 2010. The model for each day was run twice at 04:00 and 16:00 UTC.

3.3. Back Trajectory Analysis

[17] In addition to weather condition analyses, we also simulated the air-mass backward trajectories at an altitude of 500 m above sea level using the NOAA HYSPLIT model to identify the likely source regions of the two AD events and the transport paths of dust parcels during the sampling periods, as illustrated in Figure 6 for the MAD (14–16 March 2010) and Figure 7 for the SAD (20–22 March 2010). Each event was analyzed for three successive days, and each day was run twice at 04 and 16 UTC for the MAD, and 02 and 14 UTC for the SAD.

[18] On 14 March, the air masses collected at the four sites were mainly of maritime origin (Figure 6a), resulting in low Al concentrations (Figure 4). On 15 March, when Al concentration was up to higher than 3000 ng/m^3 at PCY (Figure 4), the dust-carried air masses that invaded PCY later in the day could be traced back to the Gobi and Mongolian deserts (Figure 6b) [*Zhang et al.*, 2003a, 2003b]. The Badain Juran desert was the most likely source, especially for the dust transported southeastward [*Hsu et al.*, 2008; *Liu et al.*, 2009]. In the ensuing day (16 March), when the dust plume had

Figure 7. (a–c) The NOAA HYSPLIT modeled 5 day backward trajectories at 500 m starting from the four TSP sampling stations (PCY, KM, ZH, and DS) between 20 and 22 March 2010. The model for each day was run twice at 02:00 and 14:00 UTC.
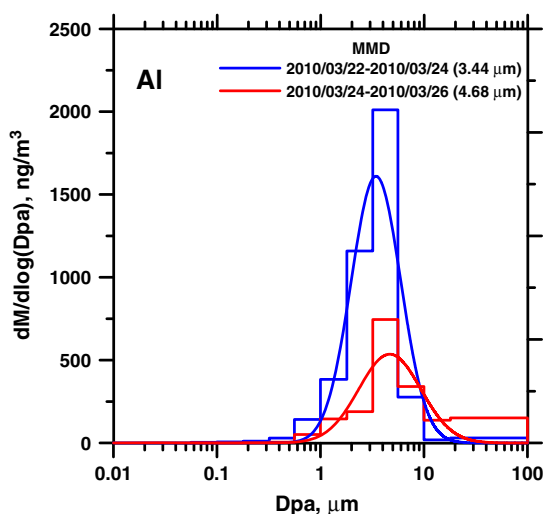
Figure 8. Size distribution of dust-derived Al in the two sets of size-resolved aerosols (stepped chart). Also shown are the log-normal fitting curves.

arrived at the other three sites, the tracked dust source was the Gobi deserts somewhere along the border between north China and Outer Mongolia, where dust phenomena have been recorded by surface observation (Figures 5b and 5c).

[19] On 20 March, the dominant origin of the air masses sampled at our four stations appeared to be maritime in nature, as the trajectories occupied the wide oceans (Figure 7a) during the modeled days. The trajectories were coupled with the time series of PM_{10} that remained at low levels on that day (Figure 3). However, they seemed inconsistent with the temporal variation in Al concentration that had increased in the samples collected at PCY and KM on 20 March. The reason is that data on Al concentration can provide only the daily time resolution, which is too low to capture the exact time of arrival of dust plumes, as described in the earlier section. The air masses sampled at PCY and KM on 21 March were clearly traced back to North China and Mongolia within 3 days and even as far as to Siberia within 5 days. This SAD case may be categorized into the Fast and Clean Type of dust event [*Hsu et al.*, 2010b]. In contrast to that in PCY and KM, the trajectories on this day, from ZH in the Pearl River Delta (PRD) and DS in the northern SCS, were not been tracked to the East Asian dust regions. One of the likely reasons is the intrinsic uncertainty of the trajectory model [*Stohl*, 1998]. However, the most likely reason is the different transport processes (pathways) for more southeastern, downwind lands/oceans. The tongue-shaped, eastward-extended SAD clouds sustained over the western Pacific, near Eastern Taiwan, as demonstrated by the spatial distribution of satellite retrieved AOD over there [*Lin et al.*, 2012], could not stretch directly into the SCS. The further incursion to the SCS (DS) might be ascribed to the low-level northeasterlies/easterlies associated with the cold air surge [*Wang et al.*, 2011], which could serve as the agent for transporting the escaped patches of dust clouds to the SCS [*Chen et al.*, 2004], affecting the DS for about 8 h [*Wang et al.*, 2011]. Such transport is different from that in the MAD case. The SAD transport to Hong Kong and, further, to the PRD, may mainly take the path along the Taiwan Strait, as suggested by *Lin et al.* [2012].

3.4. Size Distribution of Dust Al

[20] Figure 8 shows the size distribution of Al in the two sets of size-resolved aerosol samples collected in Taipei, northern Taiwan, about 100 km downwind of the PCY. Size distribution is one of the essential factors that control the dust deposition [*Prospero et al.*, 2010], and a critical parameter in the numerical model simulation and satellite signal algorithm [*Schulz et al.*, 2012]. The corresponding total Al concentrations in the two sets of samples were 4072 and 1771 ng/m^3. Although the sampling location was on land, this area was also under frequent impact of AD and, thus, could still represent the area in characterizing the southeastward transport of AD [*Hsu et al.*, 2008; *Liu et al.*, 2009]. Obviously, the size distributions of Al in the two sets of samples showed a typical monomodal pattern, which peaked at the supermicron size, ranging from 3.2 to 5.6 μm, and were much finer than that (7 to 11 μm) observed during dusty days in Beijing [*Han et al.*, 2004]. This result agrees with our previous results observed at the same site, with an average mass median diameter (MMD) of 3.6 ± 1.2 μm (n = 9) [*Hsu et al.*, 2009a].

[21] The size distribution was fitted to a log-normal distribution curve and then separated into 100 individual size bins, each corresponding to 1% of the total mass and characterized according to particle diameter at the center ($D_{0.5\%}$, $D_{1.5\%}$, ---, $D_{99.5\%}$) [*Arimoto et al.*, 1985; *Arimoto and Duce*, 1986; *Dulac et al.*, 1989; *Zhang et al.*, 2003a]. Then, we derived the MMD for these two sets of samples: 3.4 μm during the SAD days (i.e., the first sample set) and 4.7 μm during the normal days (the second sample set) (Figure 8), both of which fell within our previous range. Notably, the dust particles from the downwind region were even finer during the course of the SAD than those during the normal post-SAD days, which might be partly due to local contributions [*Formenti et al.*, 2011]. Further considering the entire particle size distribution [*Arimoto et al.*, 1985, 1997; *Zhang et al.*, 1993, 1997; *Hsu et al.*, 2009a], we used the two-layer deposition model of *Slinn and Slinn* [1980] to calculate the dry deposition velocities (DDVs) of each of the particle size bins. Note that *GESAMP* [1989] concluded that the best estimate for the DDV should be recognized to be perhaps associated with an uncertainty of a factor of three. In the computation, the data for wind speed (10 m/s) and relative humidity (85%) provided by the Central Weather Bureau of Taiwan were based on long-term observations at PCY in the southern ECS, and the other parameters applied to this study were similar to those adopted by *Dulac et al.* [1989]. The resultant integrated DDVs averaged over the 100 bin sizes of the two sets of size-segregated samples were 0.58 and 3.69 cm/s. Surprisingly, the DDV (0.58 cm/s) for the SAD days was significantly smaller than that (~2 cm/s) usually adopted for wind-blown mineral dust in the downstream regions of dust sources [*Duce et al.*, 1991].

3.5. Unexpectedly Low-Dust Deposition

[22] During the passage of this SAD, the daily dry deposition of dust particles measured between 21 and 29 March 2010 in northern Taiwan ranged from 8 to 178 mg/m^2/d, with a mean of 50 ± 60 mg/m^2/d and a maximum of 178 mg/m^2/d on 21 March (Table 1), which is even slightly lower than the springtime mean dry deposition (~200 mg/m^2/d) to the Yellow

Table 1. Dry Deposition Flux of Insoluble Dust Particles

Start Time[a]	End Time[a]	Flux (mg/m^2/d)
2010/3/21 10:30	2010/3/22 09:20	178
2010/3/22 09:20	2010/3/23 09:30	25
2010/3/23 09:30	2010/3/24 09:40	8
2010/3/24 09:40	2010/3/25 09:50	26
2010/3/25 09:50	2010/3/26 09:25	31
2010/3/26 09:25	2010/3/26 16:40	60
2010/3/26 16:40	2010/3/29 09:50	10
	Time-weighted average	
2010/3/21 10:30	2010/3/24 21:40	62
2010/3/24 21:40	2010/3/26 16:40	35

[a]Here the time is local time (LST).

Sea [*Kai and Gao*, 2007]. The magnitude of the observed dust dry deposition was consistent with the two corresponding weekly total dust fallout fluxes (i.e., 90 mg/m^2/d on 15–22 March, and 31 mg/m^2/d on 22–29 March) that were collected during the sampling period (Table 2), guaranteeing the QA/QC of dust deposition data. The first weekly fallout sample has already collected the SAD (21 March) and MAD (15 March) events. Based on the measurements of dust fallouts during the sampling season, the flux of 15 ± 3 mg/m^2/day can be regarded as the baseline (Table 2); this value is similar to the annual average dry dust deposition (5.8 ± 1.3 g/m^2/yr, equivalent to $\sim 16 \pm 4$ mg/m^2/day) that was estimated from the dust aerosol data over the study area [*Hsu et al.*, 2009a]. Therefore, the maximum flux during the peak phase of the SAD was only about 12 times that of the baseline.

[23] As further compared with the flux (>0.4 g/m^2/week, equivalent to 57 mg/m^2/day) observed at Sapporo, Japan, in April and May 1994 [*Uematsu et al.*, 2003], our value measured on the SAD day was also consistent and was only two-fold higher. For the Sapporo dust deposition, which included both dry and wet depositions, dry deposition accounted for $\sim 60\%$ of the total deposition. In contrast, no wet deposition contributed to our maximum dust deposition, because no rain occurred during the SAD day in Taipei, Taiwan, which thus indicates exclusively dry deposition. By using model simulation, *Li et al.* [2011] estimated the dust deposition in March 2010 at about 0.5 g/m^2 over the study region, thus corresponding to around 17 mg/m^2/d, which is almost similar to the mean flux averaged throughout the spring in 2010, in Taipei (Table 2). On the other hand, in comparing the extraordinary Al concentrations (over 50,000 ng/m^3) with its baseline concentration (650 ± 510 ng/m^3) in the northeasterly monsoon, which was established from a 5 year data set [*Hsu et al.*, 2008], the enhancing factor of Al concentration even reached about 80. This concentration would be at the least doubled, when considering the longer influencing time of the SAD over the southern ECS and northern Taiwan (i.e., $\sim 25°$N). This results demonstrates that the increasing factor (~ 12) of the observed dust deposition during the peak course of the SAD was relatively much lower (even one order of magnitude lower) than that (~ 200) of the dust concentration itself. Moreover, the result that the observed increase in dust deposition was not linearly proportional to that in dust concentration further reveals that the aerosol loadings retrieved from remote sensing would be unable to accurately reflect the dust deposition [*Mahowald et al.*, 2005], especially for marginal seas. These phenomena of disproportionate increases in dust concentration and deposition have also been observed by *Skonieczny et al.* [2011], whose study was conducted

at Mbour, a coastal city in West Africa. During a strong Saharan dust storm period, the PM$_{10}$ daily concentrations increased from <100 to ~ 1600 µg/m^3, and the <30 µm-sized dust deposition fluxes increased from ~ 100 to nearly 300 mg/m^2/d (as shown in their Figure 2).

[24] The dry deposition flux (F_P) of aerosol particles to the water surface can be expressed as the product of DDV (V_d) and concentration (C_P) in the boundary layer [*Duce et al.*, 1991; *Zhang et al.*, 1997], thus:

$$F_P = C_P \times V_d$$

[25] Accordingly, DDV (V_d) represents the proportionality between the flux (F_P) and the concentration (C_P), although it would be a function of complex factors [*Seinfeld and Pandis*, 2006]. Therefore, the DDV (Vd) of aerosol dust during the SAD day can be alternatively estimated from the dust dry deposition (178 mg/m^2/day) divided by the dust concentration, where the dust concentration used (730 µg/m^3) was converted from Al concentration measured at PCY during the SAD day. In accordance with the method of *Hsu et al.* [2009a], the Al concentration was converted to dust concentration by dividing it with 0.07, because the Al content in AD was assumed to be 7%, similar to that in the northern China desert dust [*Zhang et al.*, 2003a]. Consequently, the resulting DDV of dust particles only reached 0.28 cm/sec. Furthermore, we calculated the time-weighted mean dust dry deposition fluxes during the periods corresponding to the two sets of size-resolved aerosol samples: 62 and 35 mg/m^2/d (Table 1). Then, we estimated the average dry deposition velocities to be 0.24 and 1.16 cm/sec, respectively, from the observed dry dust deposition fluxes and Al concentrations (21191 and 2408 ng/m^3; equivalent to dust concentrations, 303 and 34 µg/m^3), so that we could compare the DDVs obtained by the two independent means based on the size distribution spectrum of eolian dust (as shown in the former section) and on direct observation (i.e., dry dust deposition flux and atmospheric dust concentration).

[26] The DDV results of the long-range transported dust from the two independent means were roughly comparable to one another (i.e., 0.24 versus 0.58 cm/s and 1.16 versus 3.69 cm/s), varying with a factor of about three. This result reveals that the DDV value was lower than that (~ 2 cm/s) usually applied in the literature and that (~ 1.2–3.7 cm/s) on the ensuing days of the SAD. On the other hand, the difference in the DDV values of the two means might be partly due to the difference in the exact sampling periods of each sample used. More importantly, during the peak time of the SAD, strong winds of 5–8 m/s (Figure 5h), which were much higher than normal (<3 m/s), may have caused strong mixing at the boundary layer. In turn, this mixing may have enhanced the friction velocity, which led to an increase in upward flux and a decrease in the downward flux of aerosol particles [*Goossens*,

Table 2. Bulk Deposition Flux of Insoluble Dust Particles

Start Time[a]	End Time[a]	Flux (mg/m^2/d)
2010/3/1 09:05	2010/3/8 09:30	15
2010/3/8 09:30	2010/3/15 10:00	12
2010/3/15 10:00	2010/3/22 09:20	90
2010/3/22 09:20	2010/3/29 10:00	31
2010/3/29 10:00	2010/4/6 09:50	17

[a]Here the time is local time (LST).

2008]; these factors must be considered in the model simulation to improve the modeling performance. *Maring et al.* [2003] suggested that an upward velocity of ~0.33 cm/s must be subtracted from the vertical velocity of long-range transported dust particles that are theoretically derived from the Stokes gravitational settling velocity, because of the change in the size distribution from source to the downwind.

[27] Our results definitely demonstrate that the dry deposition velocity of eolian dust is disproportionately small during strong dust episodes, thus leading to the resulting low deposition. On the other hand, numerical model simulations have obtained considerably incomparable results of dust deposition to the study oceans. For example, *Park et al.* [2011] have simulated the mean monthly dust deposition of 2331 mg/m^2/mon (i.e., 75 mg/m^2/d) to the Yellow Sea, 2221 mg/m^2/mon (i.e., 72 mg/m^2/d) to the East Sea (also called as Sea of Japan), 1454 mg/m^2/mon (i.e., 47 mg/m^2/d) to the northwest Pacific (30°N–40°N, 140°E–150°E), 695 mg/m^2/mon (i.e., 22 mg/m^2/d) to the ECS, and only 26 mg/m^2/mon (i.e., 0.8 mg/m^2/d) to the SCS, wherein the deposition to the northwest Pacific is over twofold of that to the ECS. In contrast, *Li et al.* [2011] obtained a rather uniform distribution of dust dry deposition, ranging from 0.5 to 1 g/m^2/mon (16–32 mg/m^2/d) to the Yellow Sea and ECS during March 2010; however, dust wet deposition to the same region is relatively variable, with a wide range of 0.1–5 g/m^2/mon (3–160 mg/m^2/d). For the northwest Pacific, the dust deposition is similar to the ECS, but with about half of the amount of dry deposition to the ECS. Another modeling study, namely *Tan et al.* [2012], have simulated the total dust deposition in the spring between 2000 and 2007, yielding 58, 30, 7, and 21 g/m^2/season (630, 326, 76, and 228 mg/m^2/d) for the Bohai Sea, the Yellow Sea, the ECS, and the northern SCS, respectively. Noticed that the deposition to the northern SCS is three times of that to the ECS. The inconsistency between modeling results have highlighted the importance of filed observations not only on dust concentration but also on dust deposition, which would be very helpful in the validation of modeling performance. Our results might further imply that the west Pacific other than the East Chinese marginal seas (including the Bohai, Yellow, and East China Seas, as well as the Sea of Japan) could serve as one of main receptacles of AD [*Tan et al.*, 2012]. Specifically, long-range transported AD during episodic dust events may have more extensive influence over the Northwestern Pacific, in spatial and temporal extents than conventionally thought. These results can be further verified using the spatial distribution of CALIPSO lidar data [*Lin et al.*, 2012], as earlier mentioned. Extensively distributed dust would affect the oceanic biogeochemistry and the direct and indirect radiative forcing.

4. Concluding Remarks

[28] Our results prove that, in some cases, atmospheric transport could be relatively more significant than dust strength, in relation to the southeastward transport of AD to the SCS. The increase in dust deposition during the SAD event was disproportionate, in terms of increase in dust concentration, which can be attributed to the relatively finer size of eolian dust with low dry deposition velocity. Surprisingly, the velocity (i.e., 0.2 to 0.6 cm/sec) of dust particles during the dust episode was much lower than that (1 to 2 cm/sec) usually adopted. Because our sampling location is located downwind, the AD sources and the eolian dust collected has crossed over the wide ocean, therefore it might be somewhat analog to the open ocean case, allowing broader applications. Accordingly, this phenomenon would also have implications for unraveling paleoclimate from cored sediments during the glacial time, when much stronger dust storms were believed to have been experienced compared with those of the present day (if deposited eolian dust is used as a paleoclimatic proxy). Other implications are that dust deposition cannot be accurately predicted by satellite-derived AOD and that the dispersion and ultimate sink of AD must be identified, which requires further field investigations. The spatial extent of the SAD dispersion is expected to be more extensive. The further seaward-advected SAD clouds could be removed, possibly by wet deposition, instead of dry deposition. The reason could be that dust deposition to the remote open oceans is dominated by wet deposition [*Zhao et al.*, 2003].

[29] Fe/Al ratios measured during the cause of the SAD remained constant at 0.61 ± 0.05 (Figure 4), which is very close to those of the Chinese desert and loess dust [*Zhang et al.*, 1997, 2003a], as well as those of marine aerosols collected over the ECS [*Hsu et al.*, 2010b, 2010c]. This result indicates the domination of eolian dust as iron source during the dusty period. In addition, the deposition of dust-bearing bioavailable dissolved iron to remote oceans will be more complicated, because the relative significances of synoptic atmospheric conditions and dust strength were poorly identified, apart from various controlling factors of dust iron dissolution [*Baker and Croot*, 2010; *Hsu et al.*, 2010b; *Li et al.*, 2012]; the involvement of anthropogenic sources of aerosol iron could be another complicating factor [*Luo et al.*, 2008].

References

Arimoto, R., R. A. Duce, B. J. Ray, and C. K. Unni (1985), Atmospheric trace elements at Enewetak Atoll: 2. Transport to the ocean by wet and dry deposition, *J. Geophys. Res.*, *90*, 2391–2408.

Arimoto, R., and R. A. Duce (1986), Dry deposition models and the air/sea exchange of trace elements, *J. Geophys. Res.*, *91*, 2787–2792, doi:10.1029/JD091ID02P02787.

Arimoto, R., B. J. Ray, N. F. Lewis, and U. Tomza (1997), Mass-particle size distributions of atmospheric dust and the dry deposition of dust to the remote ocean, *J. Geophys. Res.*, *102*, 15,867–15,874, doi:10.1029/97JD00796.

Aumont, O., L. Bopp, and M. Schulz (2008), What does temporal variability in aeolian dust deposition contribute to sea-surface iron and chlorophyll distributions? *Geophys. Res. Lett.*, *35*, L07607, doi:10.1029/2007GL031131.

Azimi, S., A. Ludwig, D. R. Thévenot, and J.-L. Colin (2003), Trace metal determination in total atmospheric deposition in rural and urban areas, *Sci. Total Environ.*, *308*, 247–256.

Baker, A. R., and P. L. Croot (2010), Atmospheric and marine controls on aerosol iron solubility in seawater, *Mar. Chem.*, *120*(1–4), 4–13.

Bishop, J. K. B., R. E. Davis, and J. T. Sherman (2002), Robotic observations of dust storm enhancement of carbon biomass in the North Pacific, *Science*, *298*, 817–821.

Chen, J. P., et al. (2004), Simulations of Asian yellow dust incursion over Taiwan for the spring of 2002 and 2003, *Terr. Atmos. Ocean. Sci.*, *15*, 949–981.

Chen, S. H., S. H. Wang, and M. Waylonis (2010), Modification of Saharan air layer and environmental shear over the eastern Atlantic Ocean by dust-radiation effects, *J. Geophys. Res.*, *115*, D21202, doi:10.1029/2010JD014158.

Chi, K. H., S. C. Hsu, S. H. Wang, and M. B. Chang (2008), Increases in ambient PCDD/F and PCB concentrations in Northern Taiwan during an Asian dust storm episode, *Sci. Total Environ.*, *401*, 100–108.

Choi, J. C., M. Lee, Y. Chun, J. Kim, and S. Oh (2001), Chemical composition and source signature of spring aerosol in Seoul, Korea, *J. Geophys. Res.*, *106*, 18067–18074, doi:10.1029/2001JD900090.

Chou, C. C. K., C. Y. Lin, T. K. Chen, S. C. Hsu, C. S. C. Lung, S. C. Liu, and C. Y. Young (2004), Influence of long-range transported dust particles on local air quality: A case study of the Asian dust episodes in Taipei during the spring of 2002, *Terr. Atmos. Ocean. Sci.*, *15*, 881–889.

Chung, C. C., J. Chang, G. C. Gong, S. C. Hsu, K. P. Chiang, and C. W. Liao (2011), Effects of Asian dust storms on synechococcus populations in the subtropical Kuroshio Current, *Mar. Biotechnol.*, *13*, 751–763.

Draxler, R. R., and G. D. Rolph (2012), HYSPLIT (HYbrid Single-Particle Lagrangian Integrated Trajectory) Model access via NOAA ARL READY Website (http://ready.arl.noaa.gov/HYSPLIT.php). NOAA Air Resources Laboratory, Silver Spring, MD.

Duce, R. A., C. K. Unni, B. J. Bay, J. M. Prospero, and J. T. Merrill (1980), Long-range atmospheric transport of soil dust from Asia to the tropical North Pacific: Temporal variability, *Science*, *209*, 1522–1524, doi:10.1126/science.209.4464.1522.

Duce, R. A., et al. (1991), The atmospheric input of trace species to the world ocean, *Global Biogeochem. Cycles*, *5*, 193–259, doi:10.1029/91GB01778.

Dulac, F., P. Buat-Ménard, U. Ezat, A. Melki, and G. Bergametti (1989), Atmospheric input of trace metals to the western Mediterranean: Uncertainties in modeling dry deposition from cascade impactor data, *Tellus, Ser. B*, *41*, 362–378.

Fang, M., M. Zheng, F. Wang, K. S. Chim, and S. C. Kot (1999), The long range transport of aerosols from northern china to Hong Kong – A multi-technique study, *Atmos. Environ.*, *33*, 1803–1817, 1999.

Formenti, P., et al. (2011), Airborne observations of mineral dust over western Africa in the summer Monsoon season: Spatial and vertical variability of physico-chemical and optical properties, *Atmos. Chem. Phys.*, *11*, 6387–6410.

Gao, Y., R. Arimoto, R. A. Duce, D. S. Lee, and M. Y. Zhou (1992), Input of atmospheric trace elements and mineral matter to the Yellow Sea during the spring of a low-dust year, *J. Geophys. Res.*, *97*, 3767–3777.

Gao, Y., R. Arimoto, R. A. Duce, X. Y. Zhang, G. Y. Zhang, Z. S. An, L. Q. Chen, M. Y. Zhou, and D. Y. Gu (1997), Temporal and spatial distributions of dust and its deposition to the China Sea, *Tellus, Ser. B*, *49*, 172–189.

Gao, Y., Y. J. Kaufman, D. Tanré, D. Kolber, and P. G. Falkowski (2001), Seasonal distributions of aeolian iron fluxes to the global ocean, *Geophys. Res. Lett.*, *28*(1), 29–32, doi:10.1029/2000GL011926.

GESAMP, Group of Experts on Scientific Aspects of Marine Pollution (1989), The atmospheric input of trace species to the world ocean. Reports and Studies no. 38, 111 pp., World Meteorological Organization, Geneva, Switzerland.

Goossens, D. (2008), Relationships between horizontal transport flux and vertical deposition flux during dry deposition of atmospheric dust particles, *J. Geophys. Res.*, *113*, F02S13, doi:10.1029/2007JF000775.

Han, Z., et al. (2004), Model study on particle size segregation and deposition during Asian dust events in March 2002, *J. Geophys. Res.*, *109*, D19205, doi:10.1029/2004JD004920.

Han, X., C. Ge, J. Tao, M. Zhang, and R. Zhang (2012a), Air quality modeling for a strong dust event in East Asia in March 2010, *Aerosol Air Qual. Res.*, *12*, 615–628

Han, Z., J. Li, X. Xia, and R. Zhang (2012b), Investigation of direct radiative effects of aerosols in dust storm season over East Asia with an online coupled regional climate-chemistry-aerosol model, *Atmos. Environ.*, *54*, 688–699.

Hsu, S. C., S. C. Liu, C. Y. Lin, R. T. Hsu, Y. T. Huang, and Y. W. Chen (2004), Metal compositions and characterizations of PM_{10} and $PM_{2.5}$ aerosols in Taipei during the springtime, 2002, *Terr. Atmos. Ocean. Sci.*, *15*, 925–948.

Hsu, S. C., S. C. Liu, W. L. Jeng, F. J. Lin, Y. T. Huang, S. C. C. Lung, T. H. Liu, and J. Y. Tu (2005), Variations of Cd/Pb and Zn/Pb ratios in Taipei aerosols reflecting long-range transport or local pollution emissions, *Sci. Total Environ.*, *347*, 111–121.

Hsu, S. C., S. C. Liu, W. L. Jeng, C. C. K. Chou, R. T. Hsu, Y. T. Hung, and Y. W. Chen (2006), Lead isotope ratios in ambient aerosols from Taipei, Taiwan: Identifying long-range transport of airborne Pb from the Yangtze Delta, *Atmos. Environ.*, *40*, 5393–5404.

Hsu, S. C., et al. (2008), A criterion for identifying Asian dust events based on Al concentration data collected from northern Taiwan between 2002 and early 2007, *J. Geophys. Res.*, *113*, D18306, doi:10.1029/2007JD009574.

Hsu, S. C., et al. (2009a), Dust deposition to northern Taiwan and its biogeochemical implications in the East China Sea, *J. Geophys. Res.*, *114*, D15304, doi:10.1029/2008JD011223.

Hsu, S. C., S. C. Liu, Y. T. Huang, C. C. K. Chou, S. C. C. Lung, T. H. Liu, J. Y. Tu, and F. Tsai (2009b), Long-range southeastward transport of Asian biosmoke pollution: Signature detected by aerosol potassium in Northern Taiwan, *J. Geophys. Res.*, *114*, D14301, doi:10.1029/2009JD011725.

Hsu, S. C., et al. (2010a), High wintertime PM pollution over Kinmen island off southeastern China: An overview, *J. Geophys. Res.*, *115*, D17309, doi:10.1029/2009JD013641.

Hsu, S. C., et al. (2010b), Dissolution of Asian dust iron during long-range transport: Effects of atmospheric processing, transport history, and dust and sea salt loadings, *J. Geophys. Res.*, *115*, D19313, doi:10.1029/2009JD013442.

Hsu, S. C., et al. (2010c), Sources, solubility, and dry deposition of aerosol trace elements over the East China Sea, *Mar. Chem.*, *120*, 116–127.

Hsu, S. C.-A. Huh, C. Y. Chan, S. H. Lin, F. J. Lin, and S. C. Liu (2012a), Hemispheric dispersion of radioactive plume laced with fission nuclides from the Fukushima nuclear event, *Geophys. Res. Lett.*, *39*, L00G22, doi:10.1029/2011GL049986.

Hsu, S. C., et al. (2012b), Dust transport from non-East Asian sources to the North Pacific, *Geophys. Res. Lett.*, *39*, L12804, doi:10.1029/2012GL051962.

Huh, C. A., S. C. Hsu, and C. Y. Lin (2012), Fukushima-derived fission nuclides monitored around Taiwan: Free tropospheric versus boundary layer transport, *Earth Planet. Sci. Lett.*, *319–320*, 9–14.

Husar, R. B., et al. (2001), Asian dust events of April 1998, *J. Geophys. Res.*, *106*, 18,317–18,330, doi:10.1029/2000JD900788.

Inomata, Y., Y. Igarashi, M. Chiba, Y. Shinoda, H. Takahashi (2009), Dry and wet deposition of water-insoluble dust and water-soluble chemical species during spring 2007 in Tsukuba, Japan, *Atmos. Environ.*, *43*, 4503–4512.

Iwamoto, Y., et al. (2011), Biogeochemical implications of increased mineral particle concentrations in surface waters of the northwestern North Pacific during an Asian dust event, *Geophys. Res. Lett.*, *38*, L01604, doi:10.1029/2010GL045906.

Jickells, T. D., et al. (2005), Global iron connections between desert dust, ocean biogeochemistry, and climate, *Science*, *308*, 67–71.

Jurado, E., F. M. Jaward, R. Lohmann, K. C. Jones, R. Simo, and J. Dachs (2004), Atmospheric dry deposition of persistent organic pollutants to the Atlantic and inferences for the global oceans, *Environ. Sci. Technol.*, *38*, 5505–5513.

Kai, Z., and H. Gao (2007), The characteristics of Asian-dust storms during 2000–2002: From the source to the sea, *Atmos. Environ.*, *41*, 9136–9145, doi:10.1016/j.atmosenv.2007.08.007.

Kalnay, E., et al. (1996), The NCEP/NCAR 40-year reanalysis project, *Bull. Am. Meteorol. Soc.*, *77*, 437–471.

Laurent, B., B. Marticorena, G. Bergametti, and F. Mei (2006), Modeling mineral dust emissions from Chinese and Mongolian deserts, *Global Planet. Change*, *52*, 121–141, doi:10.1016/j.gloplacha.2006.02.012.

Li, J., Z. Han, and R. Zhang (2011), Model study of atmospheric particulates during dust storm period in March 2010 over East Asia, *Atmos. Environ.*, *45*, 3954–3964.

Li, J., Z. Wang, G. Zhuang, G. Luo, Y. Sun, and Q. Wang (2012), Mixing of Asian mineral dust with anthropogenic pollutants and its impact on regional atmospheric environmental and oceanic biogeochemical cycles over East Asia: A model case study of a super-duststorm in March 2010, *Atmos. Chem. Phys.*, *12*, 7591–7607, doi:10.5194/ACP-12-7591-2012.

Lin, F. J. (2007), Atmospheric transport and deposition fluxes of airborne trace elements and nutrients over the South China Sea, Taiwan National Science Council Report, 17 pages (in Chinese, with English abstract), http://ntur.lib.ntu.edu.tw/bitstream/246246/78207/1/952621Z002029.pdf

Lin, I. I., J. P. Chen, G. T. F. Wong, C. W. Huang, and C. C. Lien (2007), Aerosol input to the South China Sea: Results from the moderate resolution imaging spectro-radiometer, the quick scatterometer, and the measurements of pollution in the troposphere sensor, *Deep Sea Res. Part II*, *54*(14–15), 1589–1601.

Lin, I.-I., G. T. F. Wong, C. C. Lien, C. Y. Chien, C. W. Huang, and J. P. Chen (2009), Aerosol impact on the South China Sea biogeochemistry: An early assessment from remote sensing, *Geophys. Res. Lett.*, *36*, L17605, doi:10.1029/2009GL037484.

Lin, I. I., et al. (2011), Fertilization potential of volcanic dust in the low-nutrient low-chlorophyll western North Pacific subtropical gyre: Satellite evidence and laboratory study, *Global Biogeochem. Cycles*, *25*, GB1006, doi:10.1029/2009GB003758.

Lin, C. Y., et al. (2012), The impact of channel effect on Asian dust transport dynamics: A case in southeastern Asia, *Atmos. Chem. Phys.*, *12*(1), 271–285.

Liu, T. H., et al. (2009), Southeastward transport of Asian Dust: Source, transport and its contributions to Taiwan, *Atmos. Environ.*, *43*(2), 458–467.

Liu, Z., Q. Liu, H. C. Lin, C. S. Schwartz, Y. H. Lee, and T. Wang (2011), Three-dimensional variational assimilation of MODIS aerosol optical depth: Implementation and application to a dust storm over East Asia, *J. Geophys. Res.*, *116*, D23206, doi:10.1029/2011JD016159

Luo, C., N. Mahowald, T. Bond, P. Y. Chuang, P. Artaxo, R. Siefert, Y. Chen, and J. Schauer (2008), Combustion iron distribution and deposition, *Global Biogeochem. Cycles*, *22*, GB1012, doi:10.1029/2007GB002964.

Mahowald, N. M., et al. (2005), Atmospheric global dust cycle and iron inputs to the ocean, *Global Biogeochem. Cycles*, *19*, GB4025, doi:10.1029/2004GB002402.

Mahowald, N. M., et al. (2009), Atmospheric iron deposition: global distribution, variability, and human perturbations, *Annu. Rev. Mar. Sci.*, *1*, 245–278, doi:10.1146/annurev.marine.010908.163727.

Maring, H., D. L. Savoie, M. A. Izaguirre, L. Custals, and J. S. Reid (2003), Mineral dust aerosol size distribution change during atmospheric transport, *J. Geophys. Res.*, *108*(D19), 8592, doi:10.1029/2002JD002536.

Martin, J. H., (1990), Glacial-interglacial CO_2 change: The iron hypothesis, *Paleoceanography 5*, 1–13.

Park, S. U., A. Choe, and M. S. Park (2011), Asian dust depositions over the Asian region during March 2010 estimated by ADAM2, *Theor. Appl. Climatol.*, *105*(1–2), 129–142.

Prospero, J. M., D. L. Savoie, R. Arimoto (2003), Long-term record of nss-sulfate and nitrate in aerosols on Midway Island, 1981–2000: Evidence of increased (now decreasing?) anthropogenic emissions from Asia, *J. Geophys. Res.*, *108*(D1), 4019, doi:10.1029/2001JD001524.

Prospero, J. M., W. M. Landing, M. Schulz (2010), African dust deposition to Florida: Temporal and spatial variability and comparisons to models, *J. Geophys. Res.*, *115*, D13304, doi:10.1029/2009JD012773.

Rea, D. K. (1994), The paleoclimatic record provided by eolian deposition in the deep sea: The geologic history of wind, *Rev. Geophys.*, *32*, 159–195.

Rolph, G. D. (2012), Real-time Environmental Applications and Display sYstem (READY) Website (http://ready.arl.noaa.gov). NOAA Air Resources Laboratory, Silver Spring, MD.

Schulz, M., et al. (2012), Atmospheric transport and deposition of mineral dust to the ocean: Implications for research needs, *Environ. Sci. Technol.*, *46*, 10390–10404.

Seinfeld, J. H. and Pandis, S. N. (2006), *Atmospheric Chemistry and Physics: From Air Pollution to Climate Change*, 2nd ed., 1203 pp., John Wiley & Sons, New York, USA.

Shaw, E. C., A. J. Gabric, and G. H. McTainsh (2008), Impacts of aeolian dust deposition on phytoplankton dynamics in Queensland coastal waters, *Mar. Freshw. Res.*, *59*, 951–962, doi:10.1071/MF08087.

Singh, R. P., A. K. Prasad, V. K. Kayetha, and M. Kafatos (2008), Enhancement of oceanic parameters associated with dust storms using satellite data, *J. Geophys. Res.*, *113*, C11008, doi:10.1029/2008JC004815.

Skonieczny, C., et al. (2011), The 7–13 March 2006 major Saharan outbreak: Multiproxy characterization of mineral dust deposited on the West African margin, *J. Geophys. Res.*, *116*, D18210, doi:10.1029/2011JD016173.

Slinn, S. A., and W. G. N. Slinn (1980), Prediction for particle deposition on natural water, *Atmos. Environ.*, *14*, 1013–1016.

Stohl, A. (1998), Computation, accuracy and applications of trajectories–A review and bibliography. *Atmos. Environ.*, *32*, 947–966.

Sun, J., M. Zhang, and T. Liu (2001), Spatial and temporal characteristics of dust storms in China and its surrounding regions, 1960–1999: Relations to source area and climate, *J. Geophys. Res.*, *106*, 10,325–10,333, doi:10.1029/2000JD900665.

Tan, S. C., G. Y. Shi, and H. Wang (2012), Long-range transport of spring dust storms in Inner Mongolia and impact on the China seas, *Atmos. Environ.*, *46*, 299–308.

Tegen I., A. A. Lacis, and I. Fung (1996), The influence on climate forcing of mineral aerosols from disturbed soils, *Nature*, *380*, 419–422.

Todd, M. C., et al. (2008), Quantifying uncertainty in estimates of mineral dust flux: An intercomparison of model performance over the Bodélé Depression, northern Chad, *J. Geophys. Res.*, *113*, D24107, doi:10.1029/2008JD010476.

Trochkine, D., Y. Iwasaka, A. Matsuki, M. Yamada, Y. S. Kim, T. Nagatani, D. Zhang, G. Y. Shi, and Z. Shen (2003), Mineral aerosol particles collected in Dunhuang, China, and their comparison with chemically modified particles collected over Japan, *J. Geophys. Res.*, *108*(D23), 8642, doi:10.1029/2002JD003268.

Uematsu, M., A. Yoshikawa, H. Muraki, K. Arao, and I. Uno (2002), Transport of mineral and anthropogenic aerosols during a Kosa event over East Asia, *J. Geophys. Res.*, *107*(D7), 4059, doi:10.1029/2001JD000333.

Uematsu, M., Z. F. Wang, and I. Uno (2003), Atmospheric input of mineral dust to the western North Pacific region based on direct measurements and a regional chemical transport model, *Geophys. Res. Lett.*, *30*(6), 1342, doi:10.1029/2002GL016645.

Uno, I., K. Yumimoto, A. Shimizu, Y. Hara, N. Sugimoto, Z. Wang, Z. Liu, and D. M. Winker (2008), 3-D Structure of Asian dust transport revealed by CALIPSO lidar and a 4DVAR dust model, *Geophys. Res. Lett.*, *35*, L06803, doi:10.1029/2007GL032329.

VanCuren, R. A., and T. A. Cahill (2002), Asian aerosols in North America: Frequency and concentration of fine dust, *J. Geophys. Res.*, *107*(D24), 4804, doi:10.1029/2002JD002204.

Wai, K. M. and P. A. Tanner (2005), Relationship between ionic composition in PM_{10} and the synoptic-scale and mesoscale weather conditions in a south China coastal city: A 4-year study, *J. Geophys. Res.*, *110*, D18210, doi:10.1029/2004JD005385.

Wang, Z. F., H. Ueda, and M. Y. Huang (2000), A deflation module for use in modeling long-range transport of yellow sand over East Asia, *J. Geophys. Res.*, *105*, 26947–26959, doi:10.1029/2000JD900370.

Wang, S., J. Wang, Z. Zhou, and K. Shang (2005), Regional characteristics of three kinds of dust storm events in China, *Atmos. Environ.*, *39*, 509–520.

Wang, S. H., et al. (2011), First detailed observations of long-range transported dust over the northern South China Sea, *Atmos. Environ.*, *45*, 4804–4808.

Wang, S. H., N. C. Hsu, S. C. Tsay, N. H. Lin, A. M. Sayer, S. J. Huang, W. K. M. Lau (2012), Can Asian dust trigger phytoplankton blooms in the oligotrophic northern South China Sea?, *Geophys. Res. Lett.*, *39*, L05811, doi:10.1029/2011GL050415.

Wong, G. T. F., S. W. Chung, F. K. Shiah, C. C. Chen, L. S. Wen, and K. K. Liu (2002), Nitrate anomaly in the upper nutricline in the northern South China Sea – Evidence for nitrogen fixation, *Geophys. Res. Lett.*, *29*(23), 2097, doi:10.1029/2002GL015796.

World Meteorological Organization (WMO) (2010), Manual on the Global Observing System, Volume I, Global aspects, WMO-No. 544 (ISBN 978-92-63-10544-8) (http://www.wmo.int/pages/prog/www/OSY/Manuals_GOS.html).

Wu, J., S. W. Chung, L. S. Wen, K. K. Liu, Y. L. L. Chen, H. Y. Chen, and D. M. Karl (2003), Dissolved inorganic phosphorus, dissolved iron, and Trichodesmium in the oligotrophic South China Sea, *Global Biogeochem. Cycles*, *17*(1), 1008, doi:10.1029/2002GB001924.

Wu, C. F., I. C. Kuo, T. C. Su, Y. R. Li, L. Y. Lin, C. C. Chan, and S. C. Hsu (2010), Effects of personal exposure to particulate matter and ozone on arterial stiffness and heart rate variability in healthy adults, *Am. J. Epidemiol.*, doi:10.1093/AJE/KWQ060.

Zhang, X. Y., R. Arimoto, Z. S. An, T. Chen, G. Zhang, G. Zhu, and X. Wang (1993), Atmospheric trace elements over source regions for Chinese dust: Concentrations, sources and atmospheric deposition on the loess plateau, *Atmos. Environ., Part A*, *27*, 2051–2067.

Zhang, X. Y., R. Arimoto, and Z. S. An (1997), Dust emission from Chinese desert sources linked to variations in atmospheric circulation, *J. Geophys. Res.*, *102*, 28,041–28,047.

Zhang, X. Y., et al. (2003a), Characterization of soil dust aerosol in China and its transport and distribution during 2001 ACE-Asia: 1. Network observations, *J. Geophys. Res.*, *108*(D9), 4261, doi:10.1029/2002JD002632.

Zhang, X. Y., S. L. Gong, T. L. Zhao, R. Arimoto, Y. Q. Wang, and Z. J. Zhou (2003b), Sources of Asian dust and role of climate change versus desertification in Asian dust emission, *Geophys. Res. Lett.*, *30*(24), 2272, doi:10.1029/2003GL018206.

Zhao, T. L., S. L. Gong, X. Y. Zhang, and I. G. McKendry (2003), Modeled size-segregated wet and dry deposition budgets of soil dust aerosol during ACE-Asia 2001: Implications for trans-Pacific transport, *J. Geophys. Res.*, *108*(D23), 8665, doi:10.1029/2002JD003363.

Zhao, J., F. Zhang, Y. Xu, J. Chen, L. Yin, X. Shang, and L. Xu (2011), Chemical characteristics of particulate matter during a heavy dust episode in a coastal city, Xiamen, 2010, *Aerosol Air Qual. Res.*, *11*, 299–308.